Progress In Electromagnetics Research, Vol. 158, 49–61, 2017

Characterization and Optimization of Cylindrical Polarimetric Array Antenna Patterns for Multi-Mission Applications

Hadi Saeidi-Manesh[1, *] and Guifu Zhang[1, 2]

Abstract—The radiation characteristics of a cylindrical array antenna for Multifunction Phased Array Radar (MPAR) and terminal MPAR (TMPAR) applications are presented. A probe-fed stacked microstrip patch antenna is used for array elements. In calculations, the embedded element pattern of the patch antenna is obtained by simulation of a 5×5 element planar array. The radiation pattern of the TMPAR- and MPAR-sized cylindrical array antenna is calculated using the coherent addition method which is verified with full-wave simulation. For cross-polarization suppression, the array elements are arranged with identical 2×2 element subarrays. The radiation patterns of MPAR and TMPAR cylindrical array antennas with and without image configuration are calculated and compared. It is shown that the low cross-polarization level and azimuthally scan invariant beam characteristics can be achieved by the cylindrical array with image arrangement.

1. INTRODUCTION

There are four radar networks consisting of eight types of radar in the United States, which currently serve for weather surveillance, air-traffic control, and homeland security. All of the radars are mechanically-scanned dish antenna systems. The four networks are (1) National Weather Surveillance Radar (WSR-88D or NEXRAD); (2) Terminal Doppler Weather Radar (TDWR), (3) Airport Surveillance Radar (ASR); and (4) Air Route Surveillance Radar (ARSR). Each radar network has its own designated specifications and serves its own mission. There are overlaps and duplications for the radar's coverage and functionality as well as inefficiency in their independent operation and difficulty in data sharing. It is cost-effective and beneficial to perform all of these missions and functions within a single radar network. To serve all of the missions with a single radar network, the Multi-Function Phased Array Radar (MPAR) network is being planned and designed [1–3]. Since NEXRAD has been upgraded with dual-polarization capability, the future MPAR needs to have this capability for accurate weather measurements. MIT Lincoln Laboratory has proposed an (MPAR) system and developed an 8×8 dual-polarization MPAR panel. This radar, if completed, will utilize a four-faced planar phased array radar (PAR) antenna to cover 360 degrees in the azimuth [1]. The radiation characteristics of a radiating structure can be optimized by optimization algorithms techniques [4–8]; however, for a four-faced PAR antenna, since each face and its broadside directions are fixed, in order to scan the required space, the beam direction of each face should be steered to off-principle plane angles that cause changes in beam characteristics and polarization coupling depending on electronic beam direction [9, 10]. For instance, in [11] Lei et al. showed that the peak of a cross-polar E-field pattern of the Planar Polarimetric PAR (PPPAR) was coaxial with the copolar beam and had a peak of 12.4 dB below the copolar peak. These levels of cross-polarization are not acceptable for weather radar measurements [12]. The Cylindrical Polarimetric Phased Array Radar (CPPAR) was introduced to avoid the aforementioned deficiencies

Received 28 December 2016, Accepted 14 February 2017, Scheduled 3 March 2017

* Corresponding author: Hadi Saeidi-Manesh (hadi.saeidimanesh@ou.edu).

[1] School of Electrical & Computer Engineering, Advanced Radar Research Center (ARRC), The University of Oklahoma, USA.

[2] School of Meteorology of The University of Oklahoma, USA.

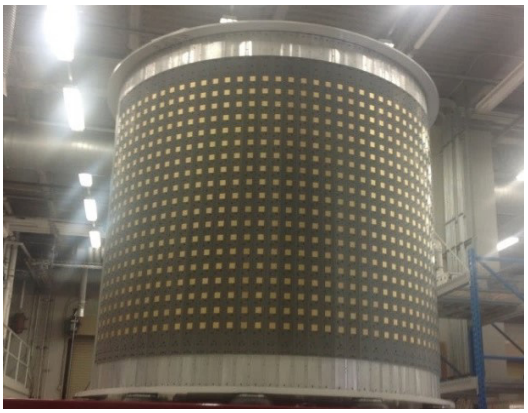

Figure 1. A picture of the OU/NSSL CPPAR demonstrator.

of PPPAR [13, 14]. A CPPAR demonstrator was designed and fabricated at the Advanced Radar Research center (ARRC) of the University of Oklahoma, in collaboration with the National Severe Storms Laboratory (NSSL), as shown in Fig. 1. The CPPAR concept has been proven to be valid and superior to the PPPAR for MPAR applications. To save costs, the CPPAR demonstrator is 2 meters in diameter and uses 96 frequency scan column antennas to cover the cylinder, making it much smaller than the real size of the MPAR or TMPAR. In this paper, further analysis and design of CPPAR for MPAR are conducted and described. In Section 2, the radiating element is designed, and its pattern characteristics are described. In Section 3, the simulation method of the MPAR-sized array with cylindrical geometry is studied by comparing the full-wave simulation results with that of coherent addition of embedded element patterns. In Section 4, the radiation patterns of MPAR- (10 m diameter) and TMPAR- (5 m diameter) sized cylindrical arrays of probe-fed and aperture-coupled patch antennas with and without image configuration are compared. The paper ends with a summary and discussion.

2. SINGLE ELEMENT DESIGN

There are many possibilities for the design of a single element in a cylindrical array antenna [15–17]. The single element used for this study is a probe-fed stack patch antenna operating at 2.7 GHz to 3 GHz [18]. The geometry of the designed element is shown in Fig. 2(b). The width of the designed square patch antenna is 55 mm. The active return loss of the designed element is shown in Fig. 2(a). This

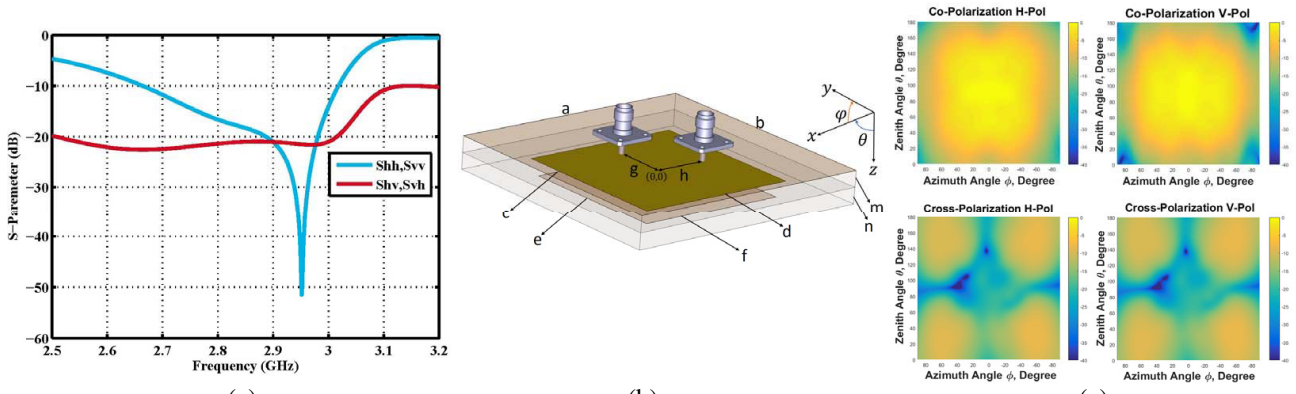

(a) (b) (c)

Figure 2. (a) Return loss and the coupling between H and V ports. (b) Single element geometry. $a = b = 50$, $c = d = 32.4$, $e = f = 30.3$, $h = g = 10.7$, $m = n = 3.175$; all dimensions are in mm. (c) Embedded element co- and cross-polarization patterns.

active S-parameter is obtained by simulation of a single element with the periodic boundary condition. The periodic boundary condition resembles the condition when all elements in the infinite array are excited, so the coupling between all elements are contributing to the resulted S-parameters. As shown in Fig. 2(a), the active S_{11} in the entire frequency band of operation is lower than -13 dB.

The embedded element pattern of the patch antenna is obtained by simulating a 5×5 element planar array antenna. The embedded element pattern is the radiation pattern of the center element while all other elements are terminated. The 2-d embedded element radiation patterns used for calculating the radiation patterns of MPAR- and the TMPAR-sized cylindrical arrays are shown in Fig. 2(c). The cross-polarization pattern in Fig. 2(c) is based on Ludwig's second definition [19]. With this definition, the spherical coordinate system does not change as the antenna rotates. In other words, when array antenna beam is steered, the coordinate system will remain fixed at the antenna location. For example, if the antenna's H port is excited, the co-polarization component will be E_φ, and the cross-polarization component will be E_θ everywhere.

3. RADIATION PATTERN OF THE CYLINDRICAL ARRAY ANTENNA

The geometry of an $M \times N$-element cylindrical array antenna is shown in Fig. 3(a). As shown in Fig. 3(a), the array consists of N, M-element linear arrays, which are placed on a circular ring with a radius of "a". Circular arrays possess the advantage of having a symmetrical radiation pattern in the azimuth, which makes the circular and cylindrical array configurations very interesting for radar applications [20]. The array radiation pattern for the circular array of radius "a" with N elements at locations $\varphi_0 = n\Delta\varphi$ can be written as:

$$E(\theta,\varphi) = \sum_{n=0}^{N-1} a_n F_n(\theta,\varphi) e^{jka\sin\theta\cos(\varphi-n\Delta\varphi)} \tag{1}$$

where a_n is the excitation coefficients of circular array elements. In general, because of symmetry, the element radiation patterns are also dependent on the element location. The effect of element location in the array can be taken into account with:

$$F_n(\theta,\varphi) = f(\theta,\varphi - n\Delta\varphi) \tag{2}$$

where $f(\theta,\varphi)$ is the embedded element radiation pattern. The radiation pattern of the cylindrical array comes from the collective contributions from the array elements on the cylindrical surface. The radiation pattern of an $M \times N$-element cylindrical array antenna when the main beam points to angle (θ_0,φ_0) can be written as:

$$E(\theta,\varphi) = e^{-j((M-1)/2)\psi_z} \sum_{m=1}^{M} e^{j(m-1)(\psi_z - kd_z\cos\theta_0)} \times \sum_{n=0}^{N-1} a_{mn} F_n(\theta,\varphi) e^{jka(\sin\theta\cos(\varphi-n\Delta\varphi) - \sin\theta_0\cos(\varphi_0-n\Delta\varphi))} \tag{3}$$

where $\psi_z = kd_z\cos\theta$ and a_{mn} is the amplitude weight applied to the mnth element of the CPPAR. The aperture distribution and excitation coefficient of cylindrical array elements can be calculated by optimization methods; however, in this paper the excitation amplitude of the mnth element is equivalent to WSR-88D illumination taper [13]:

$$a_{mn} = \frac{\left(1 - \dfrac{4\left[a^2\sin^2(\varphi_0-\varphi') + z_{mn}^2\right]}{D^2}\right)^c + b}{1+b} \tag{4}$$

where "a" for the MPAR- and TMPAR- sized array is 5 m and 2.5 m, respectively; z_{mn} is the vertical distance of mth circular array from the center of the cylindrical array; D is the height of the cylindrical array, $c = 3$, $b = 0.16$, and the MPAR (TMPAR) beam is pointed in the (θ_0,φ_0) direction.

To demonstrate the accuracy of this method for calculating the radiation pattern of the MPAR-sized cylindrical array antenna, a smaller-sized array antenna with a diameter of 1 m is simulated using HFSS [21]. The geometry of the simulated array antenna is shown in Fig. 3(b). As shown in Fig. 3(b), the simulated array is a 90-degree sector of the circular array of the designed probe-fed patch antenna.

As mentioned above, a cylindrical array is a combination of linear and circular arrays. So, instead of extending the circular array in the z direction, the periodic boundary condition is used. Also, two extra terminated elements are added to each side of this array to increase the accuracy of the simulations and reduce the edge effect error on the total radiation pattern of the array antenna. Simulations are performed under three different conditions. The first condition is that the array is a ring with the beam pointing at its broadside. The second condition is that the phase shift is applied between periodic boundaries, and the array beam axis is tilted to $(\theta_0, \varphi_0) = (80°, 0°)$. The third simulation

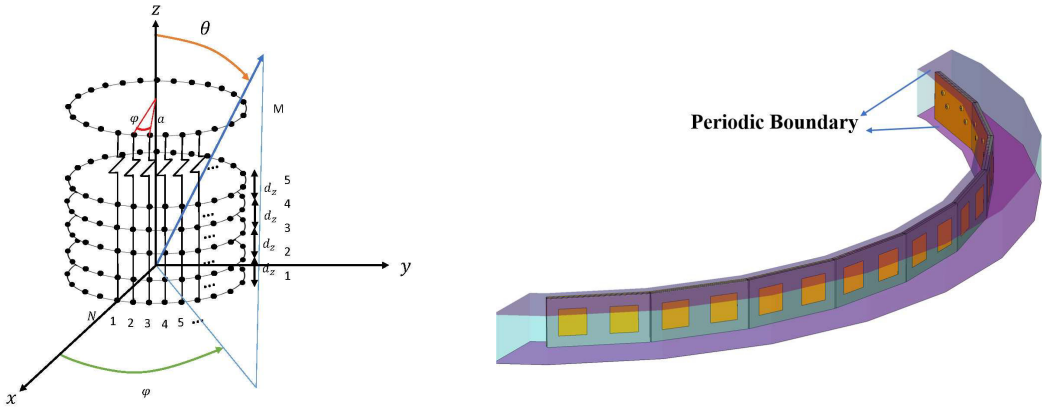

(a) (b)

Figure 3. (a) Geometry of cylindrical array antenna, (b) 90-degree sector of 64 element circular arrays. Two elements at each side are terminated.

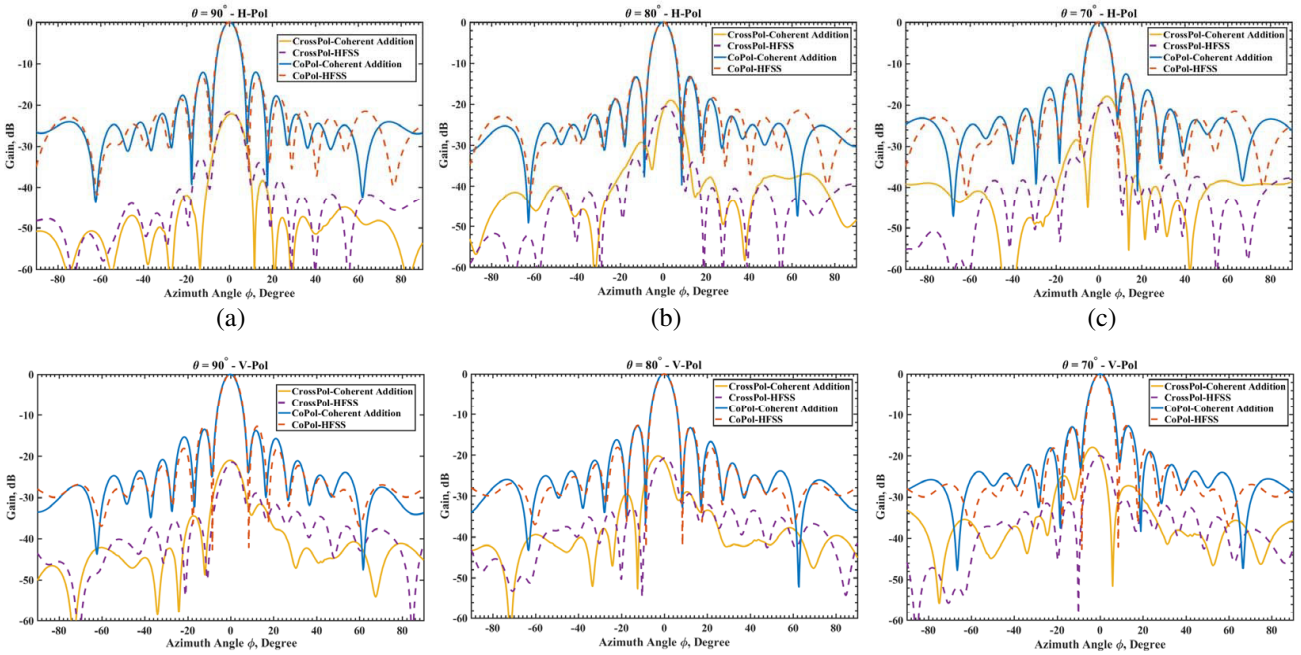

(a) (b) (c) (d) (e) (f)

Figure 4. Co-polarization and cross-polarization pattern of a 90-degree sector of a 64-element circular array calculated by full-wave simulation and coherent addition methods. (a) Horizontal polarization, $(\theta_0, \varphi_0) = (90°, 0°)$, $\theta = 90°$. (b) Horizontal polarization, $(\theta_0, \varphi_0) = (80°, 0°)$, $\theta = 80°$. (c) Horizontal polarization, $(\theta_0, \varphi_0) = (70°, 0°)$, $\theta = 70°$. (d) Vertical polarization, $(\theta_0, \varphi_0) = (90°, 0°)$, $\theta = 90°$. (e) Vertical polarization, $(\theta_0, \varphi_0) = (80°, 0°)$, $\theta = 80°$. (f) Vertical polarization, $(\theta_0, \varphi_0) = (70°, 0°)$, $\theta = 70°$.

is performed when the beam is pointed in the $(\theta_0, \varphi_0) = (70°, 0°)$ direction. The radiation pattern of the simulated array is also calculated by using an embedded element pattern. The co- and cross-polarization radiation patterns of the H and V polarizations at 2.8 GHz are calculated with the two methods (full-wave and coherent addition). These results are compared in Fig. 4. It can be seen that there is an excellent agreement between the co-polarization patterns for horizontally and vertically polarized waves in all elevation angles, as calculated by the two methods. Also, it is shown that there is a satisfactory agreement between cross-polarization patterns. Consequently, it can be concluded that coherent addition method can be used for calculating the radiation pattern of cylindrical arrays.

4. CROSS-POLARIZATION SUPPRESSION IN CYLINDRICAL ARRAY ANTENNA

Cross-polarization suppression in the dual-polarized arrays has been studied in many papers. In [22] and [18], four different arrangements for cross-polarization suppression in a dual-linear polarization array are studied. As shown in Fig. 5, there are four different arrangements based on element orientation in a 2×2 element subarray. It should be noted that configuration A is the case in which all elements are placed beside each other without any rotation. In configuration B, the two elements on the right are mirrored with respect to the vertical plane. This configuration improves the cross-polarization level in the vertical plane but causes undesirable sidelobes in the horizontal plane. In configuration C, the elements are mirrored with respect to the vertical and horizontal planes. This configuration will significantly improve the cross-polarization level in both the horizontal and vertical planes but causes undesirable sidelobes in both planes. In configuration D, the elements are mirrored with respect to the vertical planes. In this configuration, the cross-polarization is significantly improved, and the sidelobe level issue that appears in the other configurations is reduced. In configuration E, the cross-polarization is improved, especially in the main beam area, but undesirable sidelobes appear in the horizontal plane.

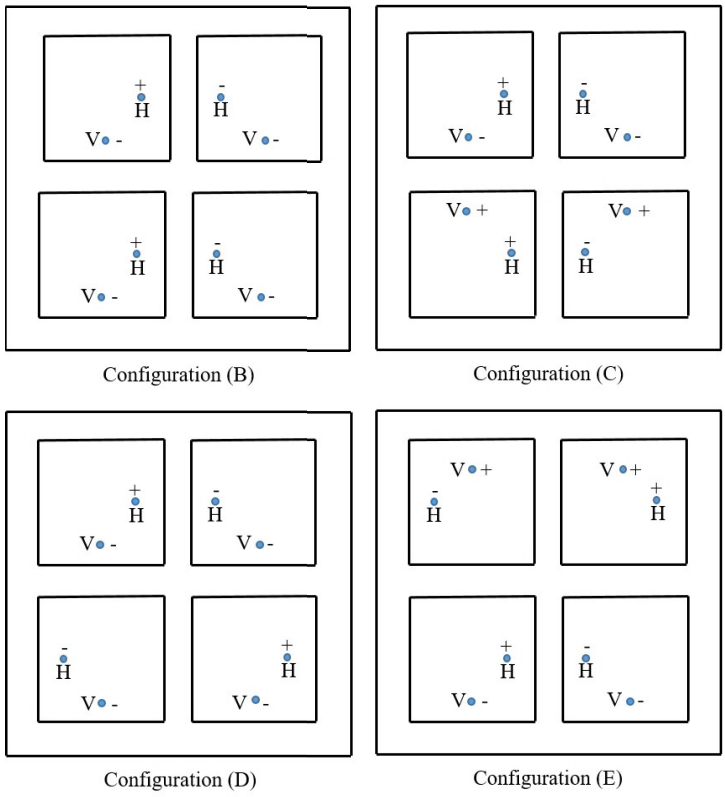

Figure 5. 2×2 element subarray configuration for cross-polarization suppression. The ports marked with "−" are excited with an 180° phase shift with respect ports marked with "+".

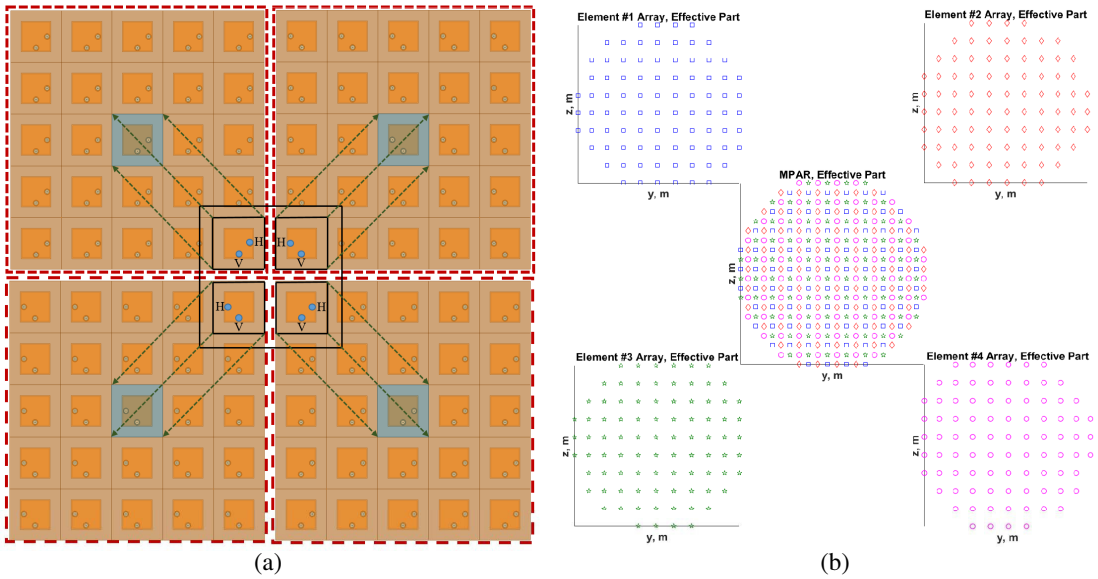

Figure 6. (a) Four 5×5 element planar array. The center element in each array is excited and all other elements are terminated to calculate the embedded element pattern. (b) The effective part of the cylindrical subarray antennas and complete cylindrical array antenna with 2×2 element subarray element.

In this paper, the elements in an MPAR-sized cylindrical array are replaced with a 2×2 element subarray arranged according to configuration D. As there are four different elements (same elements with different orientations), four different embedded element patterns are required for calculating the radiation pattern of a cylindrical array antenna with identical 2×2 element subarrays. These four embedded element patterns are calculated by simulating the four 5×5 identical element arrays, as shown in Fig. 6(a) where the elements in these arrays are the elements in the 2×2 element subarray. Simulations show that this method of calculating embedded element pattern has an acceptable accuracy for calculating the array radiation pattern. Although it is not shown, the isolation between the horizontal ports of the two top elements in 2×2 element subarray is $-22\,\text{dB}$. The isolation between horizontal ports of the two bottom elements is $-23\,\text{dB}$. This demonstrates that the orientation of elements in this design does not have a significant effect on the isolation between elements. The radiation pattern of the cylindrical array antenna is then calculated using Eq. (3). To calculate the radiation pattern of the cylindrical array with the 2×2 subarray elements, Eq. (3) should be used for each element in the 2×2 subarray separately, and the radiation patterns of all cylindrical subarrays should be combined. Also, it should be noted that the subarray location should be taken into account when using Eq. (3). As shown in Fig. 6(b), the array can be split into four different cylindrical subarrays in which each cylindrical subarray is created from identical elements. In addition, the excitation coefficients of each cylindrical subarray cannot be calculated separately. The element weights should be calculated when all the elements in the array are present, and then the weights of the four cylindrical subarrays can be extracted. The weighting matrix is calculated for the complete array and is then split into four matrices in which each matrix is used for one cylindrical subarray, depending on the location of the element in a 2×2 element subarray.

The total radiation pattern of the array, using configuration D for the 2×2 element subarrays, for horizontal polarization can be obtained by the following equations:

$$AF_{q,n}(\theta,\varphi) = e^{-j((M-2)/2)kd_z\cos\theta}\sum_{m=1}^{M} a_{q,mn}e^{j(2\times m-2)kd_z\cos\theta} \tag{5}$$

$$f_{q,n}(\theta,\varphi) = AF_{q,n}(\theta,\varphi) \times e_q(\theta,\varphi) \tag{6}$$

$$f_n^H(\theta,\varphi) = f_{1,n}(\theta,\varphi) - f_{2,n}(\theta,\varphi)e^{j\psi_y} - f_{3,n}(\theta,\varphi)e^{j\psi_z} + f_{4,n}(\theta,\varphi)e^{j(\psi_y+\psi_z)} \tag{7}$$

$$f_n^V(\theta,\varphi) = f_{1,n}(\theta,\varphi) + f_{2,n}(\theta,\varphi)e^{j\psi_y} + f_{3,n}(\theta,\varphi)e^{j\psi_z} + f_{4,n}(\theta,\varphi)e^{j(\psi_y+\psi_z)} \quad (8)$$

$$F_n^{H,V}(\theta,\varphi) = f_n^{H,V}(\theta,\varphi - n\Delta\varphi) \quad (9)$$

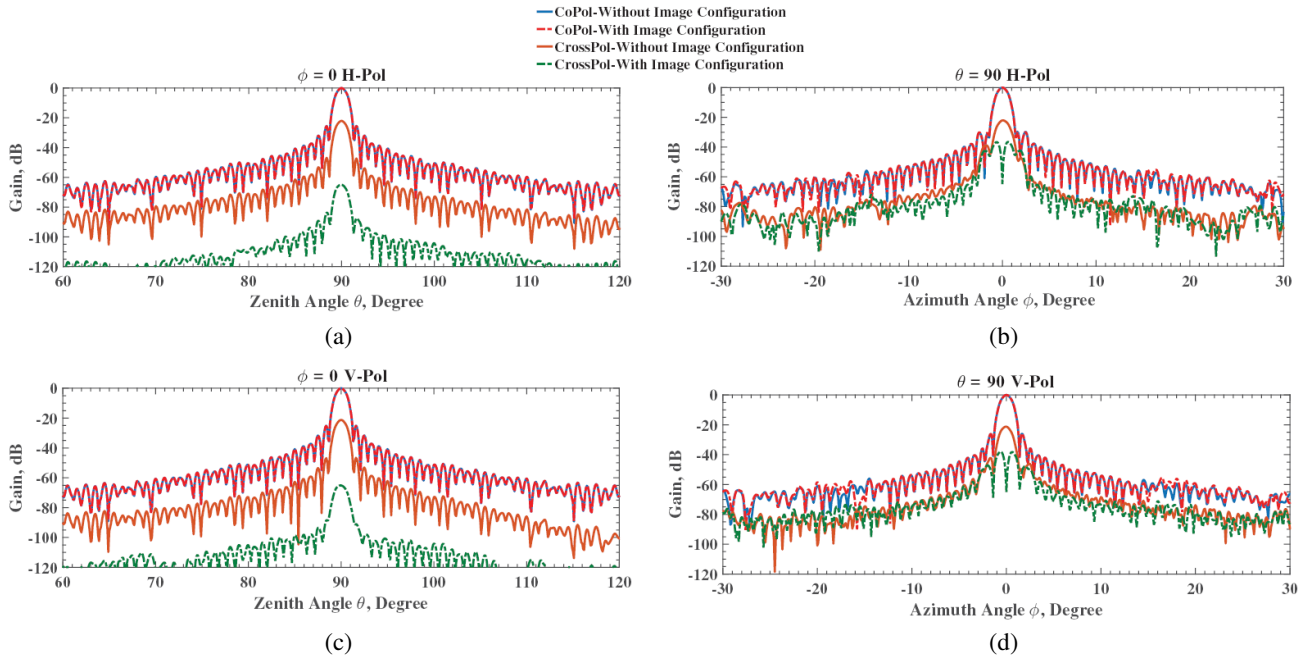

Figure 7. Co- and cross-polarization radiation patterns of MPAR. (a) Horizontal polarization, $(\theta_0,\varphi_0) = (90°,0°)$, $\varphi = 0°$. (b) Horizontal polarization, $(\theta_0,\varphi_0) = (90°,0°)$, $\theta = 90°$. (c) Vertical polarization, $(\theta_0,\varphi_0) = (90°,0°)$, $\varphi = 0°$. (d) Vertical polarization, $(\theta_0,\varphi_0) = (90°,0°)$, $\theta = 90°$.

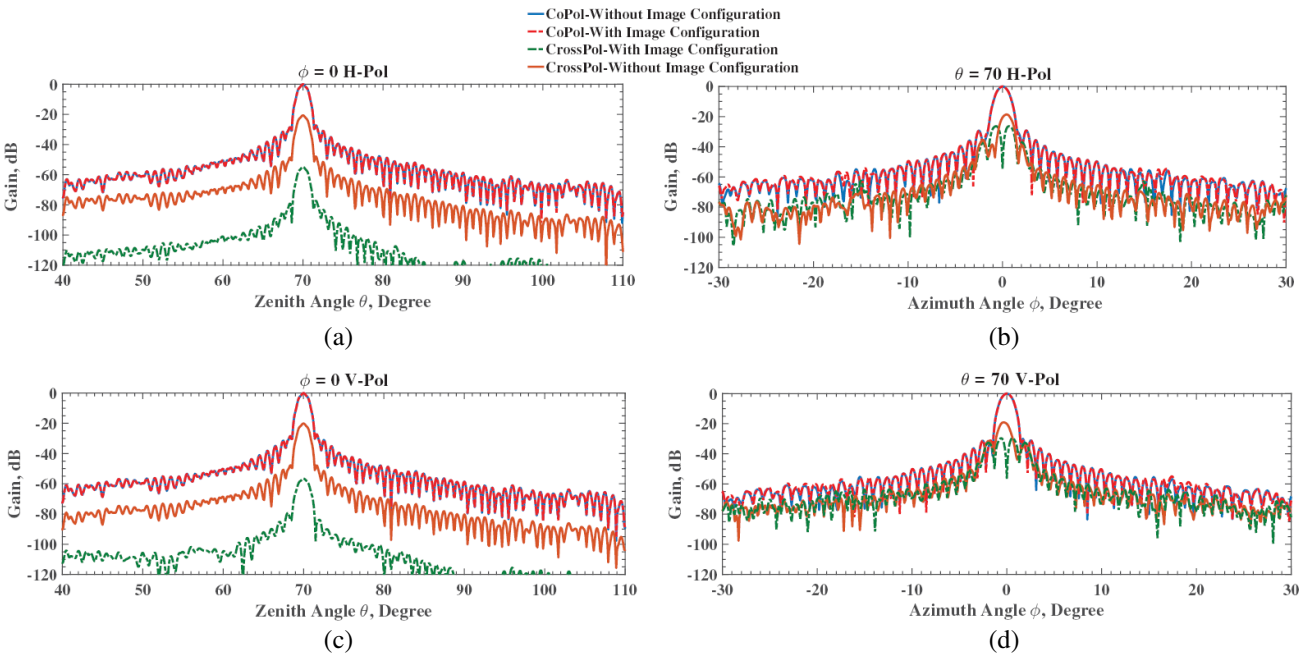

Figure 8. Co- and cross-polarization radiation patterns of MPAR. (a) Horizontal polarization, $(\theta_0,\varphi_0) = (70°,0°)$, $\varphi = 0°$. (b) Horizontal polarization, $(\theta_0,\varphi_0) = (70°,0°)$, $\theta = 70°$. (c) Vertical polarization, $(\theta_0,\varphi_0) = (70°,0°)$, $\varphi = 0°$. (d) Vertical polarization, $(\theta_0,\varphi_0) = (70°,0°)$, $\theta = 70°$.

where $AF_{q,n}(\theta,\varphi)$ is the array factor of the M-element linear array of element number q in the nth 2×2 element subarray around the circular array; $e_q(\theta,\varphi)$ is the embedded element E-field pattern of the qth element in the 2×2 subarray; $\psi_y = kd_y \sin\theta \sin\varphi$, $a_{q,mn}$ is the amplitude weights of the qth element of the 2×2 element subarray in the mnth 2×2 subarray; d_y is the spacing between elements in 2×2 element subarray. Finally, the radiation pattern of the array with image configuration can be obtained by replacing $F_n^H(\theta,\varphi)$ and $F_n^V(\theta,\varphi)$ with $a_n F_n(\theta,\varphi)$ in Eq. (1).

The broadside radiation patterns of the MPAR-sized cylindrical array with and without image configuration in the $\varphi = 0^\circ$ plane and $\theta = 90^\circ$ plane are shown in Fig. 7 and Fig. 8, respectively. As shown here, the cross-polarization levels in the horizontal and vertical polarizations are significantly improved. For horizontal polarization, the maximum cross-polarization level in $\varphi = 0^\circ$ plane is reduced from -22 dB to -65 dB, and the maximum cross-polarization level in the $\theta = 90^\circ$ plane is reduced from -22 dB to -36.6 dB.

For vertical polarization, the maximum cross-polarization level is reduced from -21.2 dB to -65 dB in $\varphi = 0^\circ$ and from -21.2 dB to -38.2 dB in $\theta = 90^\circ$. The 2-d radiation pattern of this array is shown in Fig. 9 and Fig. 10. As shown here, the maximum cross-polarization level of the array, with image configuration for horizontal polarization, is reduced from -22 dB to -36.4 dB and for vertical polarization is reduced from -21.2 dB to -38 dB.

When the array beam is pointed in $(\theta_0,\varphi_0) = (70^\circ, 0^\circ)$ direction, for horizontal polarization, the maximum cross-polarization level is reduced from -20.58 dB to -54.8 dB in the $\varphi = 0^\circ$ plane and from -18.6 dB to -26.4 dB in the $\theta = 70^\circ$ plane. For vertical polarization, the maximum cross-polarization level in the $\varphi = 0^\circ$ plane is reduced from -20.0 dB to -56.55 dB and from -19.1 dB to -29.6 dB in the $\theta = 70^\circ$ plane.

As shown in Fig. 9 and Fig. 10, when the array beam is pointed in $(\theta_0,\varphi_0) = (70^\circ, 0^\circ)$ direction, the maximum cross-polarization levels of the array with image configuration for horizontal and vertical polarizations are reduced from the -18.6 dB to -26.36 dB and from -19.1 dB to -29.6 dB respectively.

Although it is not shown here, for the TMPAR-sized cylindrical array, when the array beam is

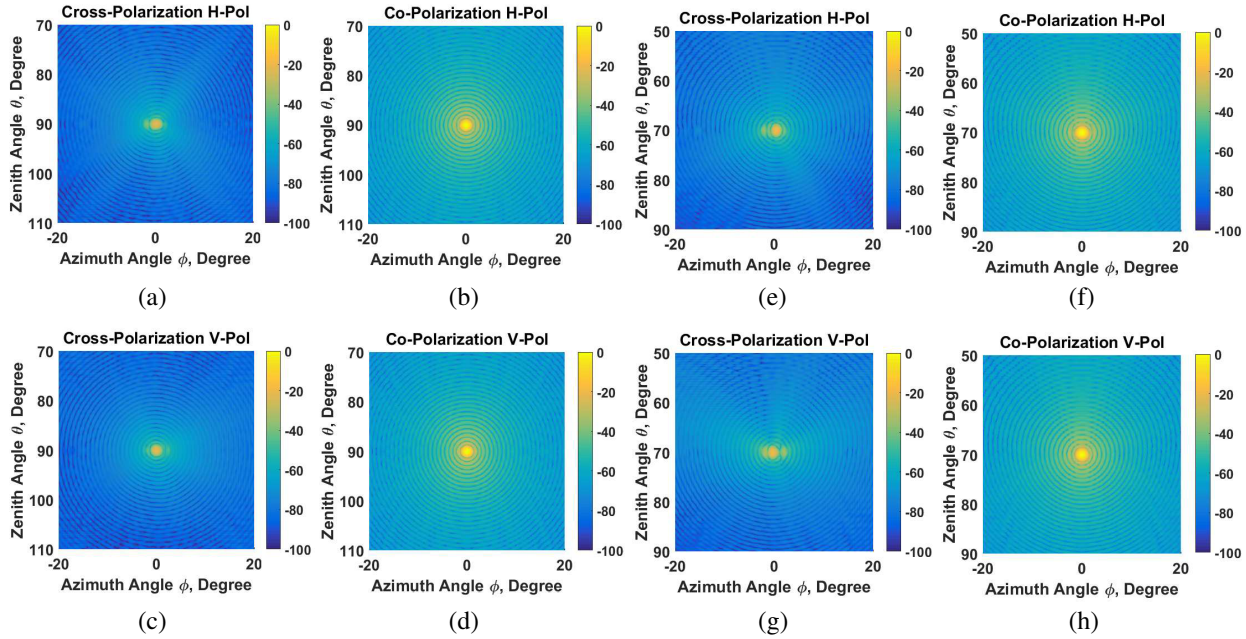

Figure 9. Co- and cross-polarization radiation patterns of MPAR without image configuration with probe-fed element. (a) Horizontal polarization, $(\theta_0,\varphi_0) = (90^\circ, 0^\circ)$, Cross-Pol. (b) Horizontal polarization, $(\theta_0,\varphi_0) = (90^\circ, 0^\circ)$, Co-Pol. (c) Vertical polarization, $(\theta_0,\varphi_0) = (90^\circ, 0^\circ)$, Cross-Pol. (d) Vertical polarization, $(\theta_0,\varphi_0) = (90^\circ, 0^\circ)$, Co-Pol. (e) Horizontal polarization, $(\theta_0,\varphi_0) = (70^\circ, 0^\circ)$, Cross-Pol. (f) Horizontal polarization, $(\theta_0,\varphi_0) = (70^\circ, 0^\circ)$, Co-Pol. (g) Vertical polarization, $(\theta_0,\varphi_0) = (70^\circ, 0^\circ)$, Cross-Pol. (h) Vertical polarization, $(\theta_0,\varphi_0) = (70^\circ, 0^\circ)$, Co-Pol.

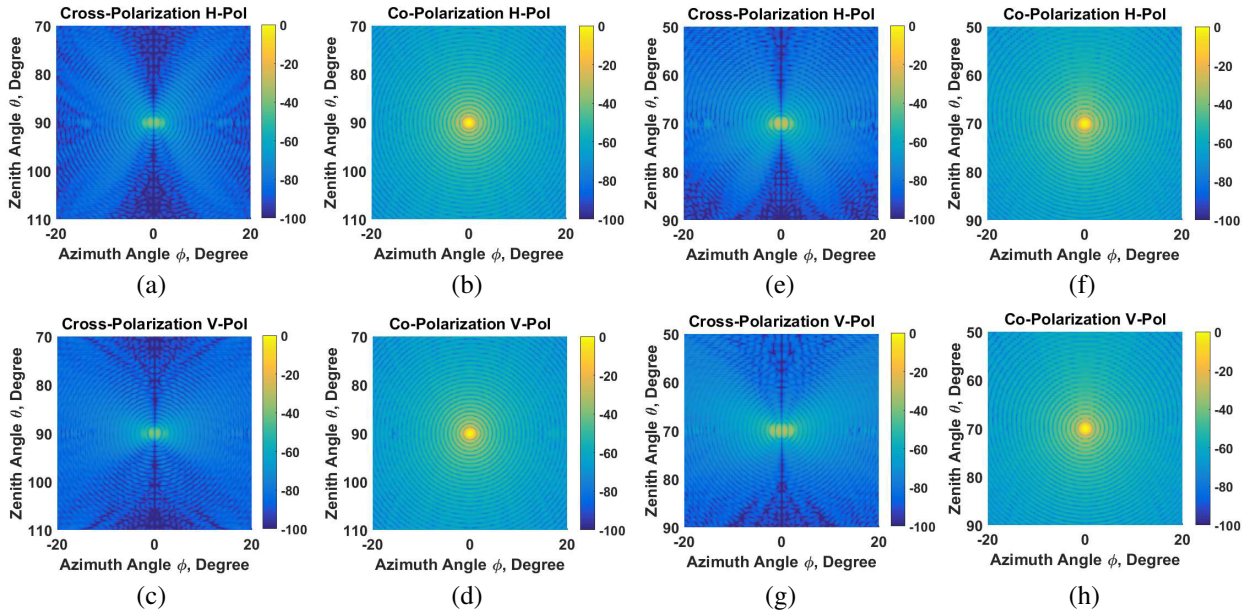

Figure 10. Co- and cross-polarization radiation patterns of MPAR with image configuration with probe-fed element. (a) Horizontal polarization, $(\theta_0, \varphi_0) = (90°, 0°)$, Cross-Pol. (b) Horizontal polarization, $(\theta_0, \varphi_0) = (90°, 0°)$, Co-Pol. (c) Vertical polarization, $(\theta_0, \varphi_0) = (90°, 0°)$, Cross-Pol. (d) Vertical polarization, $(\theta_0, \varphi_0) = (90°, 0°)$, Co-Pol. (e) Horizontal polarization, $(\theta_0, \varphi_0) = (70°, 0°)$, Cross-Pol. (f) Horizontal polarization, $(\theta_0, \varphi_0) = (70°, 0°)$, Co-Pol. (g) vertical polarization, $(\theta_0, \varphi_0) = (70°, 0°)$, Cross-Pol. (h) Vertical polarization, $(\theta_0, \varphi_0) = (70°, 0°)$, Co-Pol.

Table 1. Maximum cross-polarization level for TMPAR- and MPAR- sized cylindrical array antenna $(\theta_0, \varphi_0) = (90°, 0°)$ with probe-fed element.

Polarization	CFG-A TMPAR	CFG-D TMPAR	CFG-A MPAR	CFG-A MPAR
Horizontal	−22 dB	−36.5 dB	−22.0 dB	−36.4 dB
Vertical	−21.2 dB	−37.8 dB	−21.2 dB	−38 dB

Table 2. Maximum cross-polarization level for TMPAR- and MPAR- sized cylindrical array antenna $(\theta_0, \varphi_0) = (70°, 0°)$ with probe-fed element.

Polarization	CFG-A TMPAR	CFG-D TMPAR	CFG-A MPAR	CFG-A MPAR
Horizontal	−18.6 dB	−26.35 dB	−18.6 dB	−26.36 dB
Vertical	−19.1 dB	−29.5 dB	−19.1 dB	−29.6 dB

pointed in $(\theta_0, \varphi_0) = (90°, 0°)$ direction, the maximum cross-polarization level with image configuration is reduced from −22 dB to −36.5 dB in the horizontal polarization and reduced from −21.2 dB to −37.8 in the vertical polarization. When the array beam is pointed in $(\theta_0, \varphi_0) = (70°, 0°)$ direction, the maximum of the cross-polarization level with image configurations is reduced from −18.6 dB to −26.35 dB and from −19.1 dB to −29.5 dB in the horizontal and vertical polarizations, respectively.

Table 1 and Table 2 show the summary of the maximum cross-polarization levels with and without image configuration in the TMPAR- and MPAR-sized antennas when probe-fed patch antennas are used for array elements.

It is noted that there are two different types of cross-polarization patterns, as shown in [12]. In type-1 cross-polarization radiation pattern, the cross-polarization main lobe is coaxial with the co-

polarization main lobe. In type-2, a quad of four cross-polarization pattern peaks of alternating phase is symmetrically located about the copolar beam. As shown in Fig. 9, the radiation pattern of the cylindrical array of a probe-fed microstrip patch antenna is similar to the type-1 cross-polarization pattern. In the ideal microstrip patch antenna operating in the fundamental mode, the cross-polarization type is similar to type-2, but due to the propagation of higher order modes, the cross-polarization peak becomes coaxial with co-polarization peak. This type of cross-polarization pattern is the main cause of polarimetric parameter estimate bias, and it is thus important to change the cross-polarization from type-1 to type-2 or to suppress it. As shown in Fig. 7, the cross-polarization level in the $\varphi = 0^\circ$ plane is -65 dB, and it is totally suppressed. In $\theta = 90^\circ$ for broadside radiation and $\theta = 70^\circ$ for maximum steering angle, the cross-polarization level is reduced, and the peak of cross-polarization is transformed to a null which is deeper than -50 dB. So the image configuration not only reduces the cross-polarization level but also transforms the type-1 cross-polarization pattern to type-2, which is ideal for weather radar.

In the current version of CPPAR in ARRC, a high-performance low cross-polarization aperture coupled patch antenna is used. In this design, a dual-polarization frequency scanning array antenna is used as a column in CPPAR. In the frequency scanning array antenna, beam scanning is performed by changing the frequency of the exciter. This design eliminates the need of many phase shifters for beam steering proposes, and it is a good choice for demonstrating the idea of CPPAR. The 2-d broadside co-polarization and cross-polarization patterns of MPAR-size cylindrical array with a similar aperture coupled element used in CPPAR are shown in Fig. 11. As shown in Figs. 11(a)–(d), the maximums of cross-polarization levels for horizontal and vertical polarizations are -53.7 dB and -48.1 dB, respectively. Also, as shown in Figs. 11(e)–(h), when the array beam is pointed in $(\theta_0, \varphi_0) = (70^\circ, 0^\circ)$ direction, the maximum cross-polarization levels in the horizontal and vertical polarizations are -26.3 dB and -26.7 dB, respectively. The image configuration, which is shown to have a significant effect on cross-polarization level, is also applied on the cylindrical array with aperture coupled elements. Fig. 12 shows that, with image configuration for horizontal polarization, the broadside cross-polarization level is reduced from -53.7 dB to -59.7 dB, and for the maximum steering angle at $(\theta_0, \varphi_0) = (70^\circ, 0^\circ)$, it is reduced from -6.3 dB to -29 dB. Although the cross-polarization level for

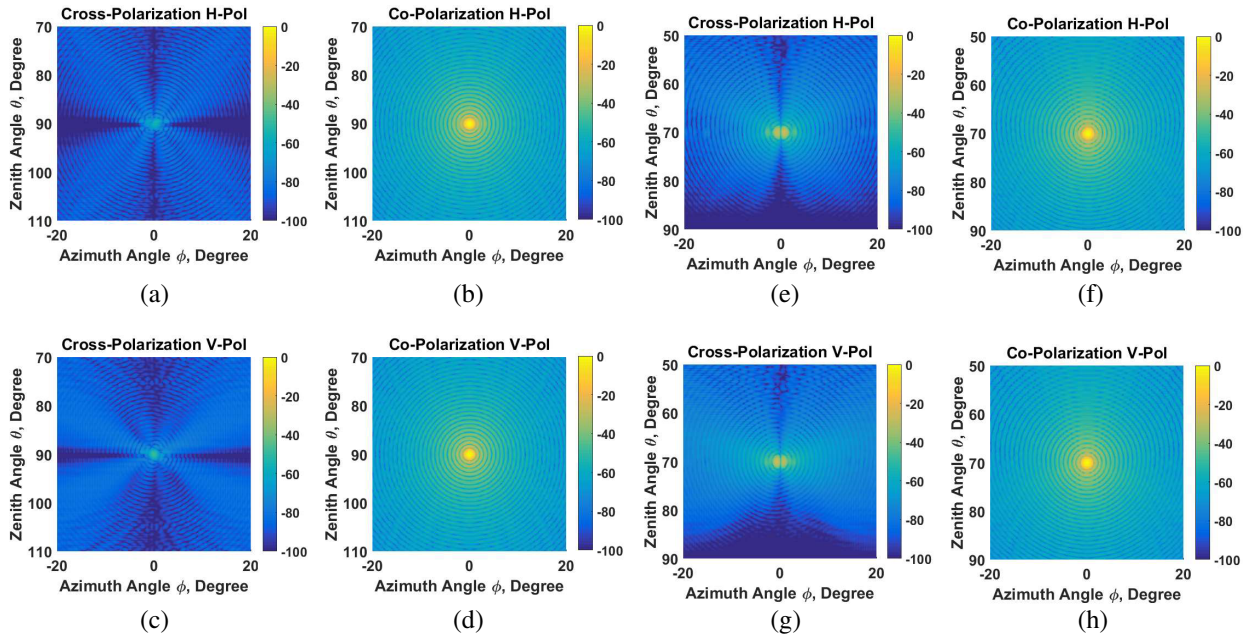

Figure 11. Co- and cross-polarization radiation pattern of MPAR without image configuration with aperture coupled element. (a) Horizontal polarization, $(\theta_0, \varphi_0) = (90^\circ, 0^\circ)$, Cross-Pol. (b) Horizontal polarization, $(\theta_0, \varphi_0) = (90^\circ, 0^\circ)$, Co-Pol. (c) Vertical polarization, $(\theta_0, \varphi_0) = (90^\circ, 0^\circ)$. Cross-Pol, (d) Vertical polarization, $(\theta_0, \varphi_0) = (90^\circ, 0^\circ)$, Co-Pol. (e) Horizontal polarization, $(\theta_0, \varphi_0) = (70^\circ, 0^\circ)$, Cross-Pol. (f) Horizontal polarization, $(\theta_0, \varphi_0) = (70^\circ, 0^\circ)$, Co-Pol. (g) Vertical polarization, $(\theta_0, \varphi_0) = (70^\circ, 0^\circ)$. Cross-Pol. (h) Vertical polarization, $(\theta_0, \varphi_0) = (70^\circ, 0^\circ)$, Co-Pol.

horizontal polarization is reduced, the cross-polarization level for vertical polarization is increased from −48.1 dB to −47 dB and −26.7 dB to −24.9 dB in broadside and maximum steering angle, respectively. Table 3 and Table 4 show the summary of the maximum cross-polarization levels with and without image configuration in TMPAR- and MPAR-sized antennas when aperture coupled patch antennas are used for array elements.

Table 5 compares the best cross-polarization level at the maximum steering angle achieved when probe-fed and aperture coupled patch antennas are used. It can be seen that the maximum cross-polarization level for horizontal polarization with aperture coupled element is 2.64 dB lower than an array with probe-fed elements. On the other hand, the maximum cross-polarization level for vertical polarization with aperture couple element is 2.9 dB higher than the results achieved by probe-fed

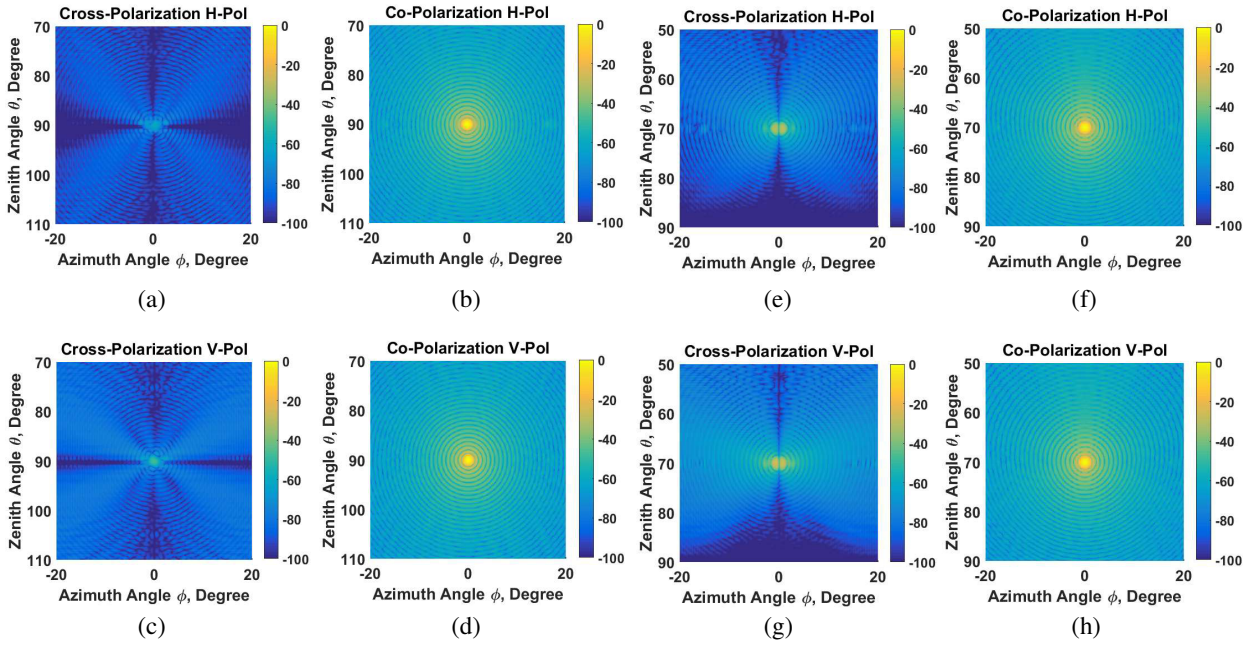

Figure 12. Co- and cross-polarization radiation pattern of MPAR with image configuration with aperture coupled element. (a) Horizontal polarization, $(\theta_0, \varphi_0) = (90°, 0°)$, Cross-Pol. (b) Horizontal polarization, $(\theta_0, \varphi_0) = (90°, 0°)$, Co-Pol. (c) Vertical polarization, $(\theta_0, \varphi_0) = (90°, 0°)$, Cross-Pol. (d) Vertical polarization, $(\theta_0, \varphi_0) = (90°, 0°)$, Co-Pol. (e) Horizontal polarization, $(\theta_0, \varphi_0) = (70°, 0°)$, Cross-Pol. (f) Horizontal polarization, $(\theta_0, \varphi_0) = (70°, 0°)$, Co-Pol. (g) Vertical polarization, $(\theta_0, \varphi_0) = (70°, 0°)$, Cross-Pol. (h) Vertical polarization, $(\theta_0, \varphi_0) = (70°, 0°)$, Co-Pol.

Table 3. Maximum cross-polarization level for MPAR- sized cylindrical array antenna $(\theta_0, \varphi_0) = (90°, 0°)$ with aperture coupled element.

Polarization	CFG-A MPAR	CFG-D MPAR
Horizontal	−53.7 dB	−59.7 dB
Vertical	−48.1 dB	−47.0 dB

Table 4. Maximum Cross-polarization level for MPAR- sized cylindrical array antenna $(\theta_0, \varphi_0) = (70°, 0°)$ with aperture coupled element.

Polarization	CFG-A MPAR	CFG-D MPAR
Horizontal	−26.3 dB	−29.0 dB
Vertical	−26.7 dB	−24.9 dB

Table 5. Lowest cross-polarization level of MPAR achieved by using probe-fed and aperture coupled element $(\theta_0, \varphi_0) = (70°, 0°)$.

Polarization	Probe-Fed	Aperture-Coupled
Horizontal	-26.3 dB	-29.0 dB
Vertical	-29.6 dB	-26.7 dB

elements. Theses results show that an array of a simple probe-fed patch antenna with image feed configuration has a better performance than an array of low cross-polarization patch antenna, and this method can eliminate the need for designing complex expensive elements for the cylindrical array antennas.

5. CONCLUSION

The radiation patterns of MPAR- and TMPAR- sized cylindrical array antennas are studied by the full-wave and coherent addition methods. The coherent addition method results are compared with full-wave simulation results, showing that excellent agreement between co-polarization patterns and satisfactory agreement between cross-polarization results are achieved. The radiation patterns of MPAR- and TMPAR-sized cylindrical array antennas with the probe-fed elements are calculated. The embedded element pattern of a 2×2 element subarray is calculated and used for calculating the radiation pattern of a cylindrical array antenna with image configuration. The coherent addition method is extended for cylindrical array antenna with identical 2×2 element subarray. The simulation results for MPAR and TMPAR array antennas with probe-fed elements and applying image configuration can significantly improve the cross-polarization level, especially in the principle plane. In addition to improving the cross-polarization level, image configuration changes the cross-polarization pattern type from type-1 to type-2 to effectively reduce bias in polarimetric parameter estimates. The cross-polarization level is also calculated when an aperture-coupled element is used. Simulation results show that the cross-polarization level for horizontal polarization is significantly improved. However, it is increased for vertical polarization. The best cross-polarization levels achieved with or without image configuration for the probe-fed patch and aperture-coupled patch antennas at a maximum steering angle are compared, showing that the array of probe-fed patch antenna has a slightly better performance. This shows the importance of the cross-polarization suppression method, which can improve the performance of the simple low-cost patch antenna and reduce the need for high-performance and high-cost radiating elements.

ACKNOWLEDGMENT

The work was supported by NOAA Grants NA11OAR4320072 and NA16OAR4320115.

REFERENCES

1. Weber, M., J. Cho, J. Flavin, J. Herd, and M. Vai, "Multifunction phased array radar for us civil-sector surveillance needs," *32nd Conf. on Radar Meteorology*, Albuquerque, New Mex., Oct. 24–29, 2005.
2. Zrnic, D., J. Kimpel, D. Forsyth, A. Shapiro, G. Crain, R. Ferek, J. Heimmer, W. Benner, T. McNellis, and R. Vogt, "Agile-beam phased array radar for weather observations," *Bulletin of the American Meteorological Society*, Vol. 88, No. 11, 1753, 2007.
3. Zhang, G., *Weather Radar Polarimetry*, CRC Press, 2016.
4. Azaro, R., F. G. De Natale, M. Donelli, A. Massa, and E. Zeni, "Optimized design of a multifunction/multiband antenna for automotive rescue systems," *IEEE Transactions on Antennas and Propagation*, Vol. 54, No. 2, 392–400, 2006.

5. Donelli, M., I. J. Craddock, D. Gibbins, and M. Sarafianou, "A three-dimensional time domain microwave imaging method for breast cancer detection based on an evolutionary algorithm," *Progress In Electromagnetics Research M*, Vol. 18, 179–195, 2011.
6. Franceschini, G., M. Donelli, R. Azaro, and A. Massa, "Inversion of phaseless total field data using a two-step strategy based on the iterative multiscaling approach," *IEEE Transactions on Geoscience and Remote Sensing*, Vol. 44, No. 12, 3527–3539, 2006.
7. Donelli, M., "Design of broadband metal nanosphere antenna arrays with a hybrid evolutionary algorithm," *Optics Letters*, Vol. 38, No. 4, 401–403, 2013.
8. Donelli, M. and P. Febvre, "An inexpensive reconfigurable planar array for wi-fi applications," *Progress In Electromagnetics Research C*, Vol. 28, 71–81, 2012.
9. Doviak, R. and D. Zrnic, "Doppler radar and weather observations academic," San Diego, Calif, 1993.
10. Karimkashi, S. and G. Zhang, "An optimal design of a cylindrical polarimetric phased array radar for weather sensing," *Radio Science*, Vol. 47, No. 2, 2012.
11. Lei, L., G. Zhang, R. J. Doviak, and S. Karimkashi, "Comparison of theoretical biases in estimating polarimetric properties of precipitation with weather radar using parabolic reflector, or planar and cylindrical arrays," *IEEE Transactions on Geoscience and Remote Sensing*, Vol. 53, No. 8, 4313–4327, 2015.
12. Zrnic, D., R. Doviak, G. Zhang, and A. Ryzhkov, "Bias in differential reflectivity due to cross coupling through the radiation patterns of polarimetric weather radars," *Journal of Atmospheric and Oceanic Technology*, Vol. 27, No. 10, 1624–1637, 2010.
13. Zhang, G., R. J. Doviak, D. S. Zrnic, R. Palmer, L. Lei, and Y. Al-Rashid, "Polarimetric phased-array radar for weather measurement: A planar or cylindrical configuration?" *Journal of Atmospheric and Oceanic Technology*, Vol. 28, No. 1, 63–73, 2011.
14. Lei, L., G. Zhang, and R. J. Doviak, "Bias correction for polarimetric phased-array radar with idealized aperture and patch antenna elements," *IEEE Transactions on Geoscience and Remote Sensing*, Vol. 51, No. 1, 473–486, 2013.
15. Mishra, P. K., D. R. Jahagirdar, and G. Kumar, "A review of broadband dual linearly polarized microstrip antenna designs with high isolation [education column]," *IEEE Antennas and Propagation Magazine*, Vol. 56, No. 6, 238–251, 2014.
16. Kumar, G. and K. Ray, *Broadband Microstrip Antennas*, Artech House, 2003.
17. Saidimanesh, H., M. S. Sorkherizi, S. Chamaani, and M. Kaboli, "A low cost wide band feed antenna for point-to-point WLAN applications," *2012 IEEE 9th International Conference on Communications (COMM)*, 167–169, 2012.
18. Saeidi-Manesh, H. and G. Zhang, "Dual-linear polarization phased array antenna cross-polarization suppression using a novel image configuration," *2016 IEEE International Symposium on Antennas and Propagation (APSURSI)*, 525–526, 2016.
19. Ludwig, A., "The definition of cross polarization," *IEEE Transactions on Antennas and Propagation*, Vol. 21, No. 1, 116–119, 1973.
20. Mailloux, R. J., *Phased Array Antenna Handbook*, Vol. 2, Artech House, Boston, 2005.
21. HFSS, A., "3-d electromagnetic simulation software," *Ansoft Corp.*, Pittsburgh, PA, 2009.
22. Woelder, K. and J. Granholm, "Cross-polarization and sidelobe suppression in dual linear polarization antenna arrays," *IEEE Transactions on Antennas and Propagation*, Vol. 45, No. 12, 1727–1740, 1997.